



Microstructure and Corrosion Response of Spark-Plasma-Sintered 304 Austenitic Stainless Steel Reinforced with Titanium Nitride in Chloride Environments

Samuel Olukayode Akinwamide · Babatunde Abiodun Obadele · Feyisayo Victoria Adams · Peter Apata Olubambi

Submitted: 10 February 2020 / Published online: 25 May 2020
© ASM International 2020

Abstract The replacement of carbon steel by stainless steel in industries where excellent corrosion resistance is required is currently gaining momentum. The susceptibility of titanium nitride (TiN)-reinforced austenitic stainless steel fabricated using sintering technique was investigated in ferric chloride (FeCl_3) and 3.5 wt.% NaCl. Microstructural observation of the sintered specimens from scanning electron microscope showed even dispersions of titanium nitride (TiN) in the matrix of austenitic stainless steel, which further confirmed the effectiveness of turbula mixing technique. Pitting corrosion resistance of specimens reinforced with 2 and 4 wt.% TiN was observed to show an improvement in ferric chloride solution after an immersion period of 96 h. The phases formed on the surface of the specimen after electrochemical test is presented in the X-ray diffraction analysis. The pitting corrosion of the sintered austenitic stainless steel specimens was also improved upon the addition of titanium nitride nanoparticles as confirmed from cyclic potentiodynamic polarization test results.

Keywords Austenitic stainless steel · Titanium nitride · Sodium chloride · Pitting · Nanoparticles

S. O. Akinwamide (✉) · B. A. Obadele · P. A. Olubambi
Center for Nanomechanics and Tribocorrosion, University of Johannesburg, Johannesburg, South Africa
e-mail: akinwamidekayode@gmail.com

B. A. Obadele
Department of Materials and Metallurgical Engineering,
Botswana International University of Science and Technology,
Palapye, Botswana

F. V. Adams
Department of Petroleum Chemistry, School of Arts and
Sciences, American University of Nigeria, Yola, Nigeria

Introduction

The extent of damage caused by corrosion in metallic structures is a function of condition and/or type of engineering application under which the material is utilized. In comparison with mild steel, stainless steel possesses excellent characteristics such as cryogenic toughness, attractive appearance, lower maintenance cost and improved corrosion resistance [1, 2]. The corrosion resistance of metals can be improved through the addition of alloying elements which include chromium, nickel and molybdenum through the formation of oxide layers on the surface of the metal. This property has made stainless steel a choice material in the design of various components in engineering industries, where high corrosion resistance is a required [3].

Despite the excellent attributes possessed by austenitic stainless steel, it is known to be susceptible to corrosion by pitting, which is an insidious form of corrosion that occurs in passive metals present in aggressive environments [4]. This mode of corrosion which occurs through the formation of small pits in a small confined area within the metal surface causes failure as a result of pitting corrosion resulting from the presence of sulfide ions in formed pits [5]. The formed pits are covered by corrosion products, making them undetectable in metallic structures where they are present. Pitting corrosion has been reported by several researchers to have affected most process facilities and power plants in various industries [6, 7].

The improved corrosion resistance of austenitic stainless steel has made it a candidate material in wide varieties of engineering applications where higher corrosion resistance at an elevated temperature is required. This improved corrosion resistance can be attributed to the presence of chromium in the range of 16–25% and nitrogen. However,

several studies have shown the susceptibility of austenitic stainless steel to corrosion by pitting despite its excellent corrosion resistance [8, 9]. Moreover, the concentrations of some essential alloying elements such as molybdenum and nitrogen in austenitic stainless steel can be increased with the aim of improving its resistance to pitting corrosion. Further studies have also confirmed that a higher amount of these alloying elements could have some adverse effect on its properties probably due to alteration of phase and microstructural changes [10, 11].

The application of nanoceramics as an approach to improving the corrosion resistance of metals and alloys has been a global area where various researchers have investigated. Samir [12] in his investigation reported the use of nanometric sized carbide-based crystallites produced by nanocrystalline plasma electrolytic method. Application of nanometric carbide on the surface of austenitic stainless steel was observed to improve its corrosion resistance. Shieu [13] also studied the control of corrosion resistance of TiN-coated stainless steel using a salt spray test. The result from this study showed an improvement in corrosion resistance of TiN-coated austenitic stainless steel. In another study by Hartwig et al. [14], the use of sputtered titanium dioxide thin films for protecting AISI 304 stainless steel against galvanic corrosion was investigated. Observation from this study shows an excellent corrosion resistance offered by sputtered titanium oxide films in AISI 304 stainless steel.

The primary elemental composition of titanium nitride is titanium and nitrogen. However, studies have shown an improvement in corrosion resistance to pitting corrosion through the addition of titanium as an alloying element in minute quantity [15]. The addition of higher volume can lead to the formation of new phases which are easily attacked by pitting. Titanium inhibits pitting by strengthening the passive films formed by stainless steel, thereby preventing further attack by chloride ions in the aggressive environment [16]. Nitrogen has also been reported to improve the pitting corrosion resistance of stainless steel through passive range widening [17, 18]. The formation of nitrates in stainless steel containing nitrogen promotes repassivation at pit sites through the reduction in molybdenum content where high pitting corrosion resistance is required [19].

Spark plasma sintering technique has been used extensively in the fabrication of metals, composites and ceramics through a process known as powder metallurgy [20, 21]. The starting powders are placed in a die, after which a mechanical pressure ranging between 20 and 100 MPa is applied in the vertical direction. This is followed by the application of high amperage voltage within the range of 0.5–40 kVA and a low voltage usually between 4 and 20 V to the die. The heat generated causes a spark discharge in the

voids present in-between powder particle surface. This technique is considered adequate for fabricating composites reinforced with ceramic particulates to its maximum density at a faster rate. Studies have shown that spark plasma sintering has other advantages over the conventional method of fabrication such as casting and hot pressing [22, 23]. This includes fabrication of sintered compacts at a much lower temperature with little or no pressure [24, 25] as well as control of final microstructure [26].

Despite several investigations by researchers, little or no reference is available on pitting corrosion resistance of sintered austenitic stainless steel reinforced with nanoceramics. The purpose of this study is to investigate further susceptibility of sintered 304-grade austenitic stainless steel reinforced with titanium nitride nanoparticle in chloride media and attempt to provide a new understanding of how the combination of titanium and nitrogen in titanium nitride can improve pitting corrosion resistance of sintered 304-grade austenitic stainless steel.

Experimental Procedure

304 SS (average particle size 22 μm , 97% pure, supplied by Sandvik Osprey Ltd, UK) and TiN (average particle size of 20 nm, 97% purity, supplied by Nanostructured & Amorphous Materials, Inc., USA) powders were used as the starting materials for this study. The chemical compositions of the powders are presented in Table 1.

Varying proportions of TiN powder (2, 4 and 6 vol.%) and 304L stainless steel powders were mixed in a dry environment using a T2F Turbula mixer at a mixing speed of 70 rpm for 5 h to ensure homogeneous dispersion of TiN powders into the matrix of 304L stainless steel. A Tescan scanning electron microscope (SEM) was used to examine the morphology of the admixed powders. Adequate powder size required to produce a specimen of 20 mm diameter with a thickness of 5 mm was filled into a graphite die. A graphite sheet was inserted between the plunges, powders and die to facilitate easy removal of sintered compacts after sintering. The fabrication of specimens by sintering technique was carried out in an automatically controlled spark plasma sintering machine with model number HHPD-25, manufactured in FCT Germany. Sandblasting was done to eliminate graphite depositions formed on the sintered compact surface to avoid contamination of the sintered compacts. Specimens for metallographic observations were prepared by grinding and polishing using different grits of silicon carbide and diamond suspensions of different microns, respectively, till a mirror-like surface was achieved.

The resistance of unreinforced (pure) and TiN-reinforced sintered 304L stainless steel to pitting corrosion was

Table 1 Elemental composition of starting powders

Elements	Fe	C	Cr	Ni	Mo	Si	Mn	S	P	N	Ti
304L SS	Bal	≤0.03	19	10	–	≤1	≤2	≤0.03	≤0.045	–	–
TiN	<0.001	0.03	–	<0.001	–	<0.003	–	–	–	21.91	77.83

investigated through the immersion of the specimens into a freshly prepared 6% ferric chloride (FeCl_3) solution (according to ASTM G-48 standard) [27]. All tests were conducted at ambient temperature for a period of 192 h, during which the specimens were vertically suspended in the FeCl_3 solution. This method has been reportedly used successfully by various researchers for determining the susceptibility of stainless steel specimens to pitting corrosion [28–30]. To prevent crevice corrosion, measures were taken to ensure that the specimens were not touching the base and walls of the container all through the test period. The morphology of the corrosion substrates was further investigated for pits formation using a Tescan scanning electron microscope equipped with energy-dispersive X-ray spectrometer (EDS). Prior to surface examinations of the corroded specimens, the corrosion products formed on the specimen surfaces were removed, washed in acetone before drying in the air. The XRD analysis of substrates was carried out using Panalytical X-ray diffractometer, and diffractograms obtained were carefully analyzed using X'pert Highscore software.

Cyclic potentiodynamic polarization test was conducted according to ASTM G61 to complement the immersion test. Cyclic potentiodynamic polarization technique is a rapid method qualitatively used in predicting the susceptibility of alloys to pitting and crevice corrosion. This was performed at ambient temperature using a VersaSTAT potentiostat equipped with a three-cell setup which consists of graphite counter electrode, silver/silver reference electrode filled with 3 M KCl solution and a working electrode. Before mounting, specimens were sectioned to 10 by 10 mm length, and copper wire was attached to one of its ends using an aluminum foil for accurate conductivity between the sample and the potentiostat. The test was initiated in 3.5 wt.% NaCl after the stabilization of the working electrode in a steady-state open-circuit potential (E_{OC}) conducted for 1 h. Prior to each experiment, specimens for the electrochemical test were embedded in resin, ground to 1200 grits using silicon carbide disks and polished to 1 micron using diamond suspension. The initial and vertex potential were kept at 1.0 V, while a final potential and scan rate of 1.5 V and 2 mV/s, respectively, were maintained throughout the test.

Results and Discussion

SEM morphologies of 304L austenitic stainless steel and nanostructured TiN powders are shown in Fig. 1(a) and (b), respectively. The pure 304L stainless steel and TiN powders are spherical with non-porous and agglomerated satellites sticking to particles with larger sizes. This indicates that the powder is produced via gas atomization route. Figure 1(c) and (d) shows the SEM micrographs of sintered specimens, which contains a varying proportion of TiN. A close observation shows a close bonding between the particles of the stainless steel matrix and the TiN reinforcements. It could be seen that the TiN is precipitated along the grain boundaries of the 304L stainless steel matrix. This observation could be as a result of a different temperature regime which exists between the stainless steel matrix and TiN reinforcement. A similar observation was reported in a study by Hegde et al. [31].

Further, an even distribution of TiN-reinforced powders within the matrix of stainless steel was also observed to be more predominant in the composite which contains 6% TiN reinforcement. Some large irregular pores were also found in sintered samples which could be as a result of hard TiN particles distribution within the grain boundary region of austenitic stainless steel [32]. A recent study has shown that the matrix/reinforcements interface and grain boundaries are favorable sites for the formation of new phases in sintered samples [33].

The plot of microhardness values obtained for the sintered specimens is presented in Fig. 2. The results confirmed that the addition of TiN to the matrix of austenitic stainless steel increased the microhardness value through a network of hard nitrides, which grows as pseudomorphic epitaxial layers along the boundaries of austenitic grains [34]. The hard nitrides impede the movement of dislocations, thereby improving the mechanical resistance of reinforced specimens. The highest microhardness value was however observed in the sintered 304L SS sample with 6% TiN reinforcement, while the lowest hardness value of 268 $\text{HV}_{0.1}$ was recorded in pure sintered stainless steel.

Figure 3 shows the SEM images of specimens immersed in FeCl_3 for 192 h. It is evident from microstructures that lesser pits which are almost hemispherical in shape were observed in all immersed samples, which is in accordance with an investigation by Bhandari et al. [35]. An increase in

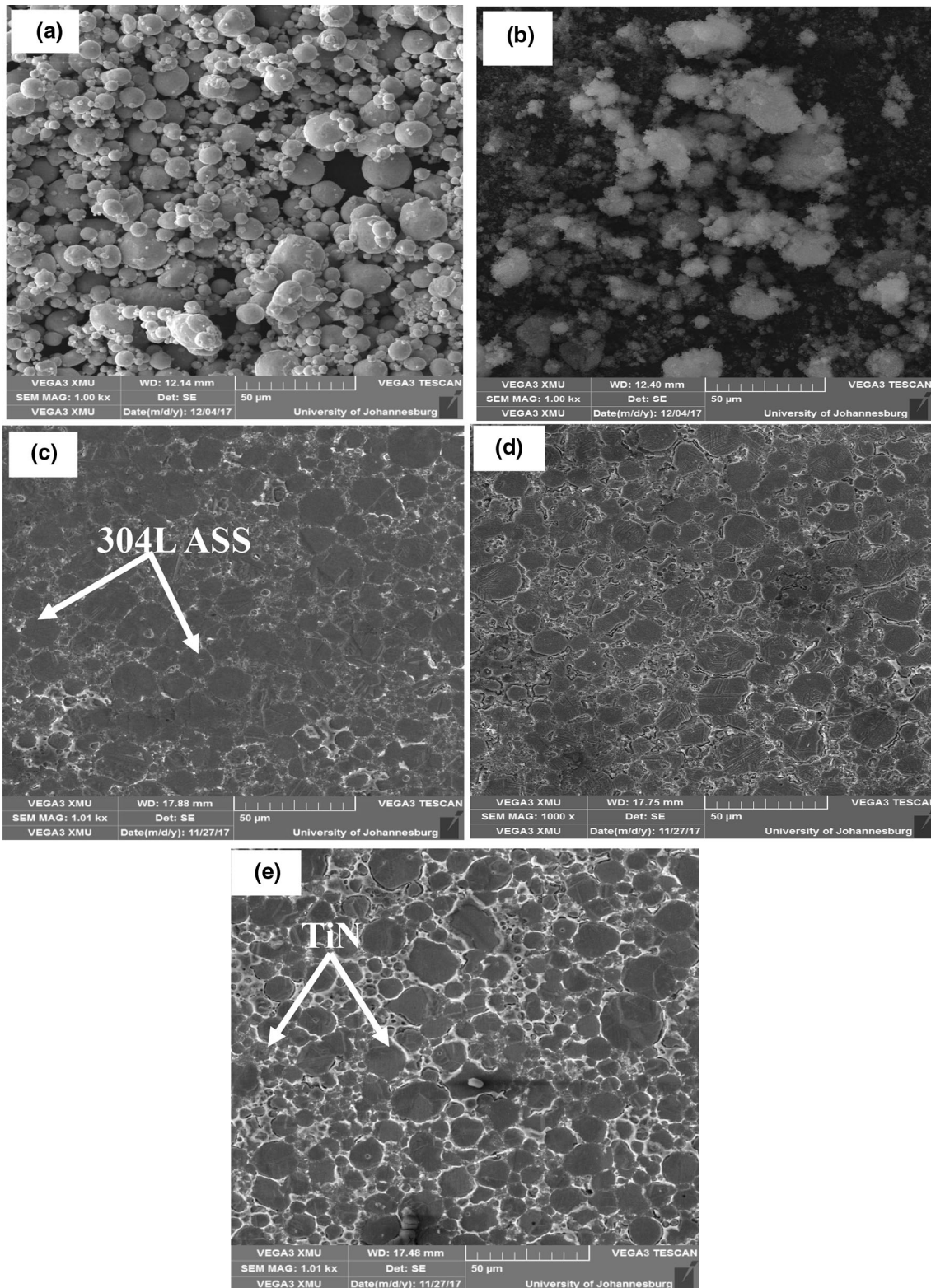


Fig. 1 SEM morphology of (a) 304L stainless steel powder, (b) TiN powder, (c) 304L SS + 2 wt.% TiN (d) 304L SS + 4% TiN and (e) 304L SS + 6% TiN

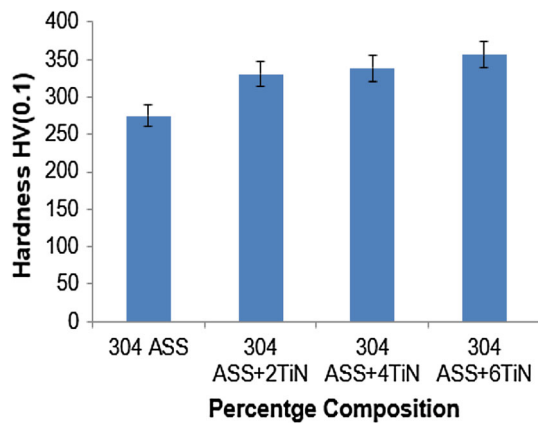


Fig. 2 Hardness plot for sintered austenitic stainless steel composites (standard errors observed were the estimate of five different indentations carried out on each sample)

immersion time shows the formation of corrosion scales, with the thinnest scale observed after 24 h of immersion. Further observation shows an increase in the thickness of corrosion scale with an increase in hours of exposure. Figure 3(a) presents the micrographs which indicate the formation of pits across the surface of pure sintered 304L stainless steel, while lesser pits are observed in Fig. 3(b) and 3(d), and no pits were visually noticed in the specimen with 4% TiN as presented in Fig. 3(c). This further confirms the resistance of this specimen to the aggressive chloride ions in the test electrolyte. However, rapid formation of pits in the specimen without TiN reinforcement could be attributed to the presence of iron (Fe) as indicated by several peaks observed in EDS analysis. The reaction between iron and oxygen in the electrolyte can promote the rate at which pits are formed in specimens. The EDS analysis of the specimen reinforced with 4% TiN shows a decrease in the peaks of Fe, while an increase is observed in the peaks of titanium (Ti) and chromium (Cr). Improved resistance to pit formation in specimens with TiN reinforcements can be ascribed to the presence of Ti and Cr in the matrix of austenitic stainless steel.

Cyclic polarization which combines both anodic and cathodic polarization to form a single cyclic process is used in evaluating the susceptibility of the specimen to pitting corrosion within a given environment. The tendency of pitting corrosion is obtained by considering the pitting potential (E_{pit}) and repassivation potential (E_{rp}). An increase in the hysteresis loop depicts higher susceptibility of the material to pitting corrosion. Pitting potential is the smallest negative potential required for pitting initiation on the surface of a metal in a passive potential region. The cyclic polarization curves for specimens are shown in Fig. 4(a–d), the pitting and passivation potentials obtained from cyclic polarization curves of specimens are presented in Table 2. The most negative value for pitting potential

was observed in the specimen with 4 wt.% TiN reinforcement, while the least negative potential was observed in pure sintered 304L sintered stainless steel. At high potentials, stainless steel is said to undergo oxygen evolution, where chromium and titanium formed become unstable [36]. This is accountable for rapid corrosion observed on the surface of the pure sintered specimen. The occurrence of pitting corrosion in specimens subjected to the corrosive medium can be ascribed to the adsorption of chloride anions on the protective layer formed on the specimen [37]. Dissolution of stainless steel occurs due to anodic overvoltage whenever there is contact between chloride ions and adsorbed oxygen, resulting in the formation of pits on the specimen surface [38]. Pits can also be formed on the specimen when there is reversible adsorption of chloride ions present in the corrosive medium. Although oxygen has a better affinity for chlorine at the adsorption site, it is reversibly adsorbed into the liquid oxygen interface, rupturing the passive protective layers formed by oxygen [39]. The improved pitting corrosion resistance observed in samples reinforced with TiN can thereby be ascribed to the protection offered by titanium and nitrogen present as the major elements in TiN utilized in reinforcing the sintered austenitic stainless steel matrix [40]. A noticeable pitting resistance observed in specimens with TiN reinforcement can also be attributed to their lower current density. The least current density was however recorded by the specimen with 4 wt.% TiN reinforcement.

Further, no current oscillation was observed in the pre-pitting potential region along the surface of TiN-reinforced composites. The breakdown of the passive layers in the specimens can be attributed to the formation of several layers of Fe_3O_4 on pre-existing chromium oxide species present in the test electrolyte. This could lead to loss of chromium oxide by dissolution through a thin pre-formed passive layer in the aqueous phase, thereby preventing the formation of a passive region in the anodic scan.

Figure 5(a) and (b) shows the SEM microstructure and EDS analysis of pure sintered austenitic stainless steel and specimen reinforced with 4% TiN. Figure 5(a) shows the presence of pit formation across the surface of pure sintered austenitic stainless steel. This could be as a result of the constant and rapid dissolution of metallic ions by adsorbed oxygen present in the corrosive medium. Pit formation was observed to reduce in specimen reinforced with 4% TiN, as shown in Fig. 5(b). The presence of chromium and titanium observed from EDS analysis played an important role in improving the corrosion resistance of the substrate. The role played by titanium, chromium and oxygen dissolution during the corrosion of stainless steel is demonstrated in the equations below [41–43].

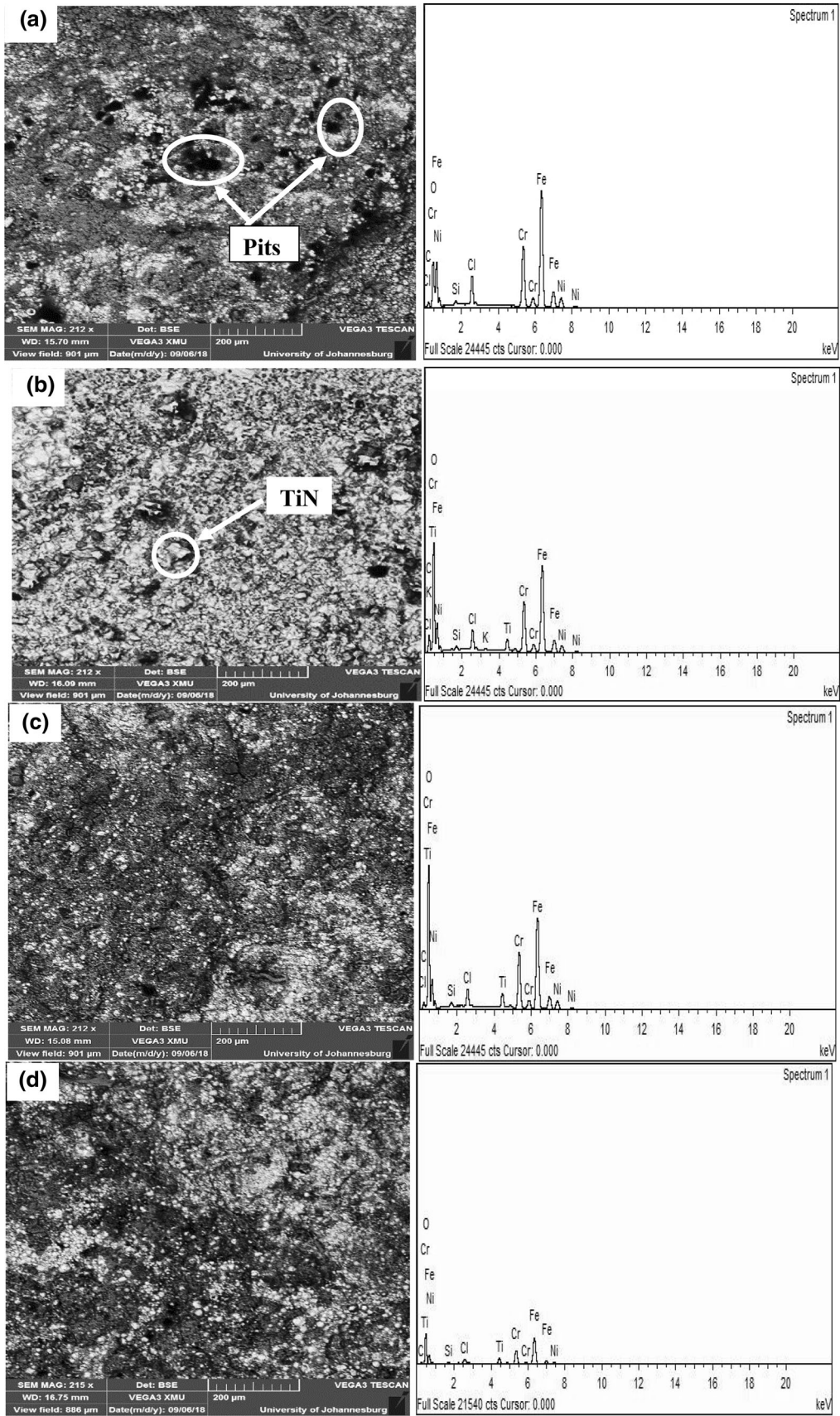
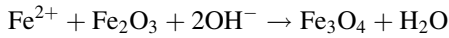
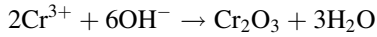
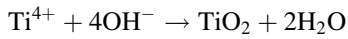
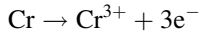
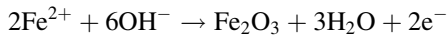


Fig. 3 SEM and EDS microstructure for (a) pure sintered 304L austenitic stainless steel (b) 304L + 2% TiN (c) 304L + 4% TiN (d) 304L + 6% TiN



During the transformation from active to a passive state, there is the formation of thick oxide layers which consists of mixed titanium and ferric oxide. These oxides help in reducing the rate at which dissolution of metal ions occurs on the surface of the substrates.

Table 2 Pitting and passivation potential for specimens

Specimen	<i>E_{pit}</i> (V)	<i>E_{rp}</i> (V)
Pure sintered 304L	− 0.105	− 0.2
Pure sintered 304L + 2% TiN	− 0.144	− 0.0152
Pure sintered 304L + 4% TiN	− 0.684	− 0.589
Pure sintered 304L + 6% TiN	− 0.448	− 0.145

The results obtained from XRD analysis were further analyzed using an X'pert Highscore software to reveal the compounds formed on the surface of the substrates, as shown in Fig. 6. Some major peaks were observed in specimens used for cyclic polarization. The peaks of Fe₃O₄ and TiSi₂ were observed to be stronger in the austenitic stainless steel specimen reinforced with 2 and 4% TiN. However, a slight phase shift in the values of 2 Θ from 49° to 50° in TiSi₂ can be attributed to the presence of silicon

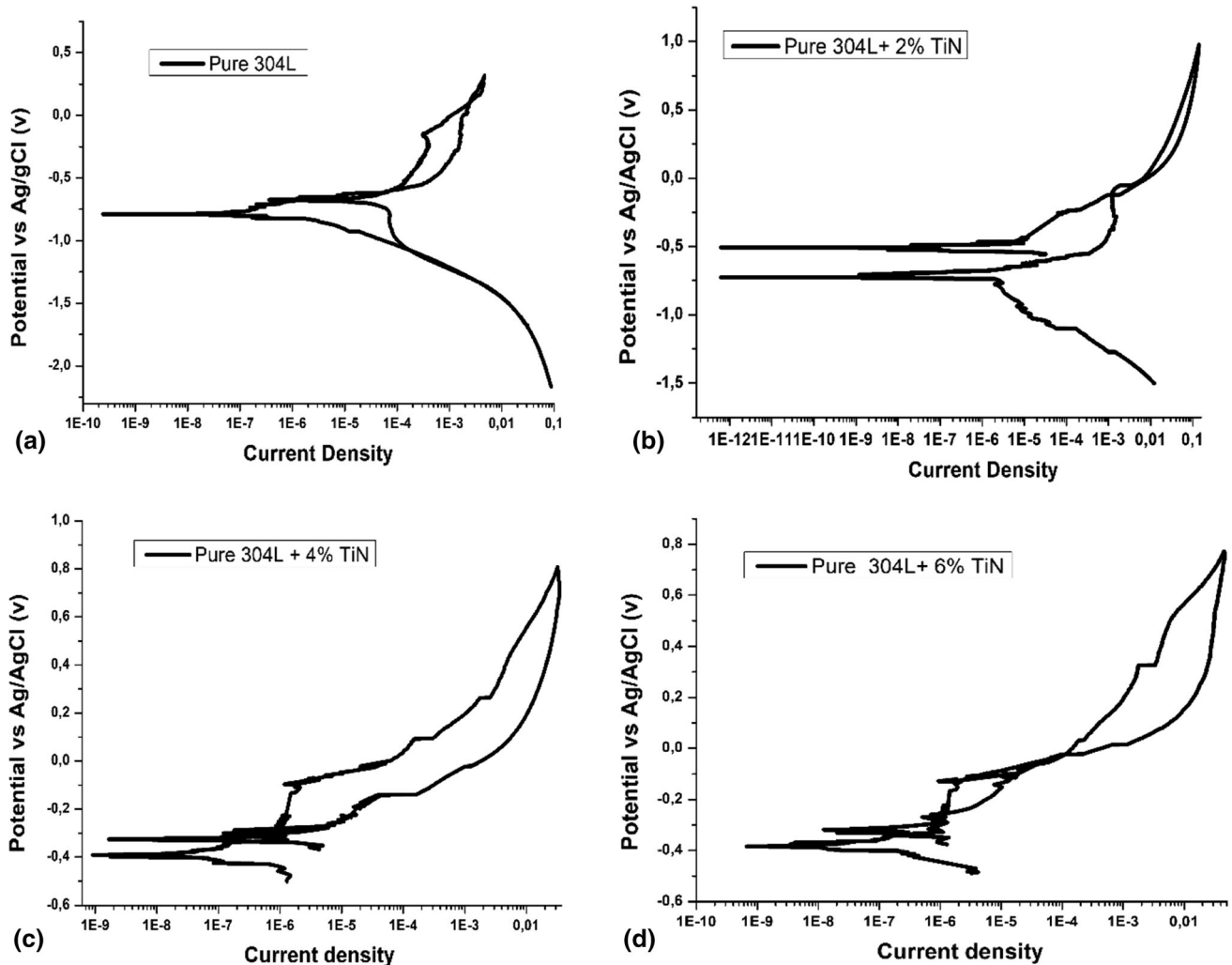


Fig. 4 Cyclic polarization curves for (a) pure sintered 304L austenitic stainless steel (b) 304L + 2 wt.% TiN (c) 304L + 4 wt.% TiN (d) 304L + 6 wt.% TiN

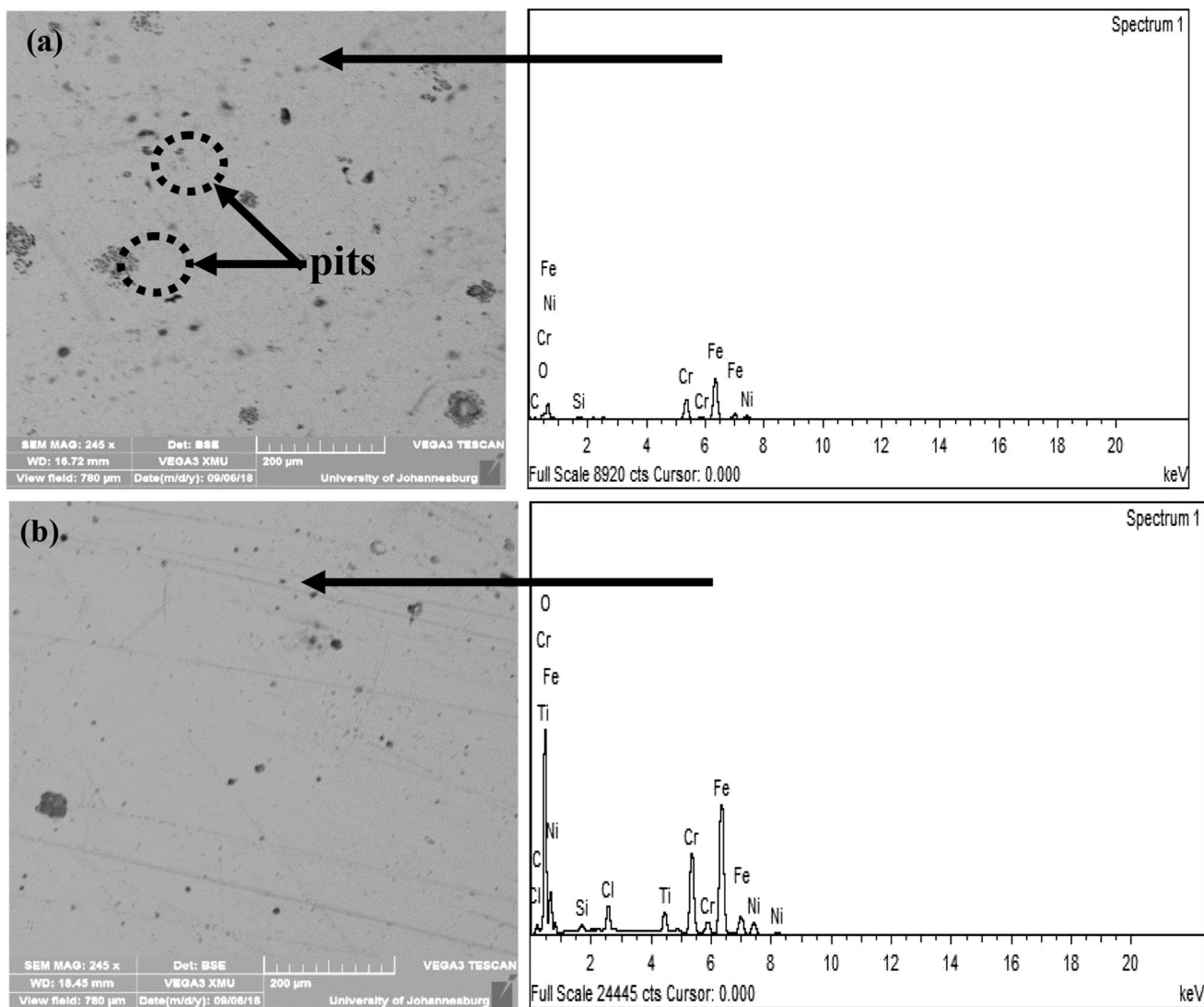


Fig. 5 SEM and EDS analysis of (a) pure sintered austenitic stainless steel (b) 304L + 4% TiN

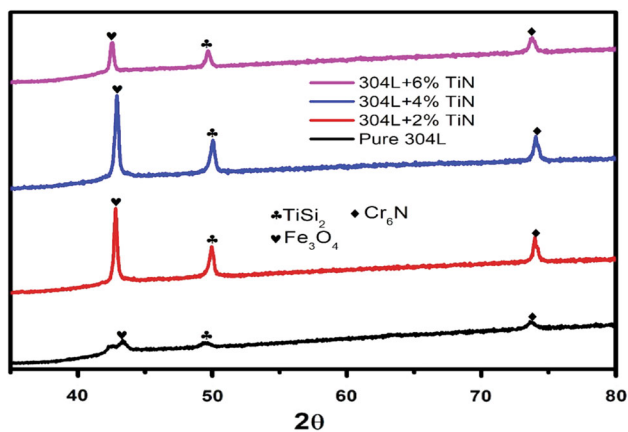


Fig. 6 XRD spectra for sintered pure and reinforced austenitic stainless steel

in the compound, as a similar trend was observed in peaks of Cr_6N . Some traces of TiO_2 and SiO_2 detected on the surface of the specimen with 2% TiN reinforcement could be the reason for its improved corrosion resistance. A similar observation was reported in a recent study by Grycova et al. [44].

Conclusion

Microstructural and pitting resistance of pure and titanium nitride-reinforced sintered austenitic stainless steel was investigated by immersion in ferric chloride and electrochemically in 3.5 wt.% NaCl. The scanning electron micrographs of the as-received TiN powder showed an agglomerated satellite-structured particle stacked together. Some irregular pores observed in sintered specimens were

as a result of TiN settling along grain boundaries of austenitic stainless steel matrix. Immersion test carried out in 6% ferric chloride for 96 h confirmed an improved corrosion resistance of specimen with 2 and 4% TiN reinforcements, while more bottomless pits were formed on the surface of pure sintered stainless steel. Similar results were further obtained in the electrochemical test conducted in 3.5 wt.% NaCl using cyclic polarization. The presence of titanium and nitrogen as the significant compositional elements was confirmed to increase the pitting resistance of TiN-reinforced specimens.

Acknowledgment The authors appreciate the Global Excellence and Stature of University of Johannesburg, South Africa and National Research Foundation, South Africa for funding this research.

References

1. B. Weiss, R. Stickler, Phase instabilities during high temperature exposure of 316 austenitic stainless steel. *Metall. Trans.* **3**, 851–866 (1972)
2. L. Gardner, The use of stainless steel in structures. *Prog. Struct. Mat. Eng.* **7**, 45–55 (2005)
3. S. Ziemiak, M. Hanson, Corrosion behavior of 304 stainless steel in high temperature, hydrogenated water. *Corros. Sci.* **44**, 2209–2230 (2002)
4. J. Bhandari, F. Khan, R. Abbassi, V. Garaniya, R. Ojeda, Modelling of pitting corrosion in marine and offshore steel structures—a technical review. *J. Loss Prev. Process Ind.* **37**, 39–62 (2015)
5. W. Tian, N. Du, S. Li, S. Chen, Q. Wu, Metastable pitting corrosion of 304 stainless steel in 3.5% NaCl solution. *Corros. Sci.* **85**, 372–379 (2014)
6. R. Murata, J. Benaquisto, C. Storey, A methodology for identifying and addressing dead-legs and corrosion issues in a Process Hazard Analysis (PHA). *J. Loss Prev. Process Ind.* **35**, 387–392 (2015)
7. A. Krzemiń, A. Więckol-Ryk, A. Smoliński, A. Koterka, L. Więclaw-Solny, Assessing the risk of corrosion in amine-based CO₂ capture process. *J. Loss Prev. Process Ind.* **43**, 189–197 (2016)
8. M.J. Jiménez-Come, E. Muñoz, R. García, V. Matres, M. Martín, F. Trujillo, I. Turias, Pitting corrosion behaviour of austenitic stainless steel using artificial intelligence techniques. *J. Appl. Logic* **10**, 291–297 (2012)
9. T. Devine, Mechanism of intergranular corrosion and pitting corrosion of austenitic and duplex 308 stainless steel. *J. Electrochem. Soc.* **126**, 374–385 (1979)
10. J. Potgieter, P. Olubambi, L. Cornish, C. Machio, E.-S.M. Sherif, Influence of nickel additions on the corrosion behaviour of low nitrogen 22% Cr series duplex stainless steels. *Corros. Sci.* **50**, 2572–2579 (2008)
11. M. Sumita, T. Hanawa, S. Teoh, Development of nitrogen-containing nickel-free austenitic stainless steels for metallic biomaterials. *Mater. Sci. Eng. C* **24**, 753–760 (2004)
12. S.M. Elsariti, M. Nazree, Nano-structure of stainless steel materials and corrosion
13. F. Shieu, Y. Sung, L. Cheng, J. Huang, G. Yu, Control of the corrosion resistance of TiN-coated AISI 304 stainless steel. *Corros. Sci.* **39**, 893–899 (1997)
14. A. Hartwig, O. Klein, H. Karl, Sputtered titanium dioxide thin films for galvanic corrosion protection of AISI 304 stainless steel coupled with carbon fiber reinforced plastics. *Thin Solid Films* **621**, 211–219 (2017)
15. P. Perillo, Corrosion behaviour of titanium nitride coating on titanium and zircaloy-4. *Am. J. Mater. Sci. Appl.* **3**, 18 (2015)
16. L. Bamoulid, M.-T. Maurette, D. De Caro, A. Guenbour, A.B. Bachir, L. Aries, S. El Hajjaji, F. Benoît-Marquié, F. Ansart, An efficient protection of stainless steel against corrosion: combination of a conversion layer and titanium dioxide deposit. *Surf. Coat. Technol.* **202**, 5020–5026 (2008)
17. H. Dong, P.-Y. Qi, X. Li, R. Llewellyn, Improving the erosion–corrosion resistance of AISI 316 austenitic stainless steel by low-temperature plasma surface alloying with N and C. *Mater. Sci. Eng. A* **431**, 137–145 (2006)
18. Y.-T. Xi, D.-X. Liu, D. Han, Improvement of corrosion and wear resistances of AISI 420 martensitic stainless steel using plasma nitriding at low temperature. *Surf. Coat. Technol.* **202**, 2577–2583 (2008)
19. W.A. Ghanem, W. Hussein, S. Saeed, S. Bader, R.A. Shahba, Effect of nitrogen on the corrosion behavior of austenitic stainless steel in chloride solutions. *Modern Appl. Sci.* **9**, 119 (2015)
20. H. Rack, Fabrication of high performance powder-metallurgy aluminum matrix composites. *Mater. Manuf. Process* **3**, 327–358 (1988)
21. J. Yan, F. Wang, K. Jiang, Y. Gu, J. Zhang, Multi-response optimisation of fabrication of 304L stainless steel/Cu composites with powder metallurgy. *Mater. Res. Innov.* **19**, S8–855 (2015)
22. C. Selcuk, S. Bond, P. Woollin, Joining processes for powder metallurgy parts: a review. *Powder Metall.* **53**, 7–11 (2010)
23. A. Tan, J. Teng, X. Zeng, D. Fu, H. Zhang, Fabrication of aluminium matrix hybrid composites reinforced with SiC microparticles and TiB₂ nanoparticles by powder metallurgy. *Powder Metall.* **60**, 66–72 (2017)
24. M. Shongwe, M. Ramakokovhu, S. Diouf, M. Durowoju, B. Obadele, R. Sule, M. Lethabane, P. Olubambi, Effect of starting powder particle size and heating rate on spark plasma sintering of FeNi alloys. *J. Alloys Compd.* **678**, 241–248 (2016)
25. X. Li, C. Liu, K. Luo, M. Ma, R. Liu, Hot deformation behaviour of SiC/AA6061 composites prepared by spark plasma sintering. *J. Mater. Sci. Technol.* **32**, 291–297 (2016)
26. L. Cheng, Z. Xie, G. Liu, W. Liu, W. Xue, Densification and mechanical properties of TiC by SPS-effects of holding time, sintering temperature and pressure condition. *J. Eur. Ceram. Soc.* **32**, 3399–3406 (2012)
27. A. G48-11, Standard test methods for pitting and crevice corrosion resistance of stainless steels and related alloys by use of ferric chloride solution (2009)
28. J. Moloney, W. Mok, C. Menendez, In situ assessment of pitting corrosion and its inhibition using a localized corrosion monitoring technique. *Corrosion* **66**, 065003–065018 (2010)
29. H. Zitter, G. Mori, G. Hochörtler, H. Wieser, Evaluation of CPT values determined by ASTM G48 practice. Report on round robin tests of the Corrosion Committee of the Austrian Society of Metallurgy. *Mater. Corros.* **53**, 37–43 (2002)
30. G. Engelhardt, D. Macdonald, Deterministic prediction of pit depth distribution. *Corrosion* **54**, 469–479 (1998)
31. M.A. Hegde, M.A. Patil, M.V. Tambrallimath, Corrosion behaviour of sintered austenitic stainless steel composites. *Int. J. Eng. Res. Technol.* **3**, 14–17 (2014)
32. S.R. Oke, O.O. Ige, O.E. Falodun, B.A. Obadele, M.B. Shongwe, P.A. Olubambi, Optimization of process parameters for spark plasma sintering of nano structured SAF 2205 composite. *J. Mater. Res. Technol.* **7**, 126–134 (2018)

33. I. Sulima, S. Boczkal, L. Jaworska, SEM and TEM characterization of microstructure of stainless steel composites reinforced with TiB₂. *Mater. Charact.* **118**, 560–569 (2016)
34. A.A. Maradudin, J.R. Sambles, W.L. Barnes, *Modern Plasmonics* (Elsevier, Amsterdam, 2014)
35. J. Bhandari, S. Lau, R. Abbassi, V. Garaniya, R. Ojeda, D. Lisson, F. Khan, Accelerated pitting corrosion test of 304 stainless steel using ASTM G48; Experimental investigation and concomitant challenges. *J. Loss Prev. Process Ind.* **47**, 10–21 (2017)
36. R.T. Loto, Pitting corrosion evaluation of austenitic stainless steel type 304 in acid chloride media. *J. Mater. Environ. Sci.* **4**, 448–459 (2013)
37. T. Hoar, D. Mears, G. Rothwell, The relationships between anodic passivity, brightening and pitting. *Corros. Sci.* **5**, 279–289 (1965)
38. H. Leckie, H. Uhlig, Environmental factors affecting the critical potential for pitting in 18–8 stainless steel. *J. Electrochem. Soc.* **113**, 1262–1267 (1966)
39. A.K. Roy, D.L. Fleming, S.R. Gordon, Effect of chloride concentration and pH on pitting corrosion of waste package container materials, in Lawrence Livermore National Lab. (1996)
40. S. Ningshen, U.K. Mudali, R. Dayal, Electrolyte and temperature effects on pitting corrosion of type 316LN stainless steels. *Br. Corros. J.* **36**, 36–41 (2001)
41. M. Sakashita, N. Sato, The effect of molybdate anion on the ion-selectivity of hydrous ferric oxide films in chloride solutions. *Corros. Sci.* **17**, 473–486 (1977)
42. J.-O. Nilsson, Super duplex stainless steels. *Mater. Sci. Technol.* **8**, 685–700 (1992)
43. J. Li, C. Du, Z. Liu, X. Li, M. Liu, Effect of microstructure on the corrosion resistance of 2205 duplex stainless steel. Part 1: Microstructure evolution during isothermal aging at 850° C and evaluation of anticorrosion properties by methods of cyclic potentiodynamic polarization and electrochemical impedance tests. *Constr. Build. Mater.* **189**, 1286–1293 (2018)
44. A. Gryčov, G. Kejmarov, J. Matoufek, Corrosion of SiO₂ and TiO₂ sol-gel layers in water and diluted HCl. *Ceramics-Silikáty* **46**, 49–51 (2002)

Publisher's Note Springer Nature remains neutral with regard to jurisdictional claims in published maps and institutional affiliations.